Minimal Assist-as-Needed Controller for Upper Limb Robotic Rehabilitation

Ali Utku Pehlivan, *Student Member, IEEE*, Dylan P. Losey, *Student Member, IEEE*, and Marcia K. O'Malley, *Senior Member, IEEE*

***Abstract*—Robotic rehabilitation of the upper limb following neurological injury is most successful when subjects are engaged in the rehabilitation protocol. Developing assistive control strategies that maximize subject participation is accordingly an active area of research, with aims to promote neural plasticity and, in turn, increase the potential for recovery of motor coordination. Unfortunately, state-of-the-art control strategies either ignore more complex subject capabilities or assume underlying patterns govern subject behavior and may therefore intervene suboptimally. In this paper, we present a minimal assist-as-needed (mAAN) controller for upper limb rehabilitation robots. The controller employs sensorless force estimation to dynamically determine subject inputs without any underlying assumptions as to the nature of subject capabilities and computes a corresponding assistance torque with adjustable ultimate bounds on position error. Our adaptive input estimation scheme is shown to yield fast, stable, and accurate measurements regardless of subject interaction and exceeds the performance of current approaches that estimate only position-dependent force inputs from the user. Two additional algorithms are introduced in this paper to further promote active participation of subjects with varying degrees of impairment. First, a bound modification algorithm is described, which alters allowable error. Second, a decayed disturbance rejection algorithm is presented, which encourages subjects who are capable of leading the reference trajectory. The mAAN controller and accompanying algorithms are demonstrated experimentally with healthy subjects in the RiceWrist-S exoskeleton.**

***Index Terms*—Adaptive control, human–robot interaction, Lyapunov methods, nonlinear control systems, rehabilitation robotics, sensorless control.**

I. Introduction

AROUND 795 000 people suffer strokes each year in the United States; the leading cause of long-term disability, stroke has broad social impacts and an estimated $33.6 billion yearly cost [1]. Spinal cord injury (SCI) incidence is approximately 12 500 each year in the United States [2], with yearly direct and indirect costs of approximately $14.5 billion and $5.5 billion [3]. Rehabilitation of patients with neurological impairments, such as stroke and SCI, primarily requires repetitive motions, which are known to improve muscle strength and movement coordination [4]. In order to increase functional outcomes and promote plasticity of the brain and spinal cord, therapy must be intensive, with long duration and high subject involvement [5].

Robotic devices are well suited for rehabilitation after stroke and SCI because they ensure the consistency of repetitive and intense therapeutic interactions. Robotic systems also enable objective and quantitative evaluations of subject performance both during and after treatment sessions. In addition, virtual reality interfaces provide unique mediums where therapy can be rendered within functional and motivational contexts [6]; consequently, the intensity of therapy can be increased. Clinical studies involving robotic rehabilitation protocols further support the implementation of these devices for the treatment of stroke [7] and SCI [8].

Control of rehabilitation robots, however, remains an open-ended research area. Assistive strategies, which target a wide range of severely to mildly impaired subjects, are the most extensively investigated controller paradigm in the rehabilitation robotics community [9] and have been shown to be the most promising techniques for promoting recovery after stroke [10]. There is strong evidence that active participation induces neural plasticity [11], and therefore, assistive controllers should intervene minimally so as to best promote involvement and recovery. Increasing treatment efficiency by minimizing robotic effort is particularly important because it reduces the overall duration and cost of intensive therapy sessions.

To address this phenomenon, several controllers have been proposed, which seek to provide minimal amounts of robotic assistance. Impedance control—as described by [12]—is frequently employed, and controller properties are modified based on subject performance. Krebs *et al.* [13] detail an impedance scheme with both a force-field tunnel normal to trajectory direction and a constant gain virtual back-wall on subject velocity. Mao and Agrawal [14] similarly utilize a force-field tunnel normal to trajectory direction, but maintain constant assistive tangential forces, which allow movement velocities to be completely defined by the subject. Mihelj *et al.* [15] include a dead-band about the desired trajectory and decrease the stiffness of an assistive virtual spring when subject error is within that dead-band.

Impedance controllers can be simply implemented and have intuitive properties; unfortunately, these control approaches fail to incorporate the time-varying capabilities of a human user and may therefore intervene incorrectly. For instance, when a

Manuscript received April 15, 2015; revised October 22, 2015; accepted October 30, 2015. Date of publication December 17, 2015; date of current version February 3, 2016. This paper was recommended for publication by Editor B. J. Nelson and Associate Editor E. Yoshida upon evaluation of the reviewers' comments. This work was supported in part by the NSF CNS-1135916, by the NSF GRFP 0940902, and by grants from Mission Connect, a project of the TIRR Foundation. *(Ali Utku Pehlivan and Dylan P. Losey contributed equally to this work.)*

The authors are with the Mechatronics and Haptic Interfaces Laboratory, Department of Mechanical Engineering, Rice University, Houston, TX 77005 USA (e-mail: aliutku@rice.edu; dlosey@rice.edu; omalleym@rice.edu).

Color versions of one or more of the figures in this paper are available online at http://ieeexplore.ieee.org.

Digital Object Identifier 10.1109/TRO.2015.2503726

subject is not able to satisfy some preset performance metric, the virtual wall defined in [13], the tangential force defined in [14], or the virtual spring defined in [15] will provide assistive efforts with constant gain control action. The subject might still be able to provide an input in the desired direction, however, and accordingly require less assistance than is provided; alternatively, the subject may atypically resist desired motions and substantially deviate from the reference trajectory.

So as to more faithfully adjust robotic assistance in response to temporal variabilities in subject performance, several adaptive control schemes have been proposed. Emken *et al.* [16] use an established model of human motor adaptation to derive an adaptive robotic controller, where assistance is reduced via a naturally inspired forgetting factor. Wei *et al.* [17] combine a feedback controller with an adaptive feedforward term—which is updated between tasks—to address consistent errors during repetitive therapeutic tasks. Conversely, Proietti *et al.* [18] introduce a controller that adaptively changes feedback gains on a task-by-task basis, effectively modulating the impedance to match subject ability.

We argue, however, that providing *minimal* assistance only becomes possible when the subject's functional capability is known; adaptive controllers that incorporate subject input estimation are often applied for this purpose. In particular, Gaussian radial basis networks have attracted considerable interest due to their universal approximation property [19]. Inclusion of Gaussian radial basis networks in adaptive control algorithms was previously proposed for both real-time robot control [20] and arm motion modeling purposes [21]. This approach fundamentally assumes subject input to be position dependent and estimates that input via Gaussian radial basis functions (RBFs) distributed throughout the workspace.

Wolbrecht *et al.* [22] first employed an adaptive controller with Gaussian RBFs for the purposes of robotic rehabilitation. To ensure continuous subject engagement, the authors include an adaption law that decreases assistive forces—i.e., "forgets" the estimated subject input—whenever tracking errors are small. This approach is problematic, however, because estimates of subject input are necessarily perturbed by the forgetting factor. Pehlivan *et al.* [23] also use RBFs, but decouple input estimation and engagement problems by directly manipulating the subject's positional error bounds. Both [24] and [25] improve the estimation ability of [22] through directionally dependent RBFs.

For a Gaussian radial basis network to accurately estimate a subject's functional capability, that subject's ability to complete tasks must be strictly a function of their position in the workspace. While this consistency may be reasonably expected from healthy individuals, it is not necessarily present in neurologically impaired subjects—consider the effects of movement disorders [26] and varying velocities [27], [28] on torque production and reaching capabilities. Furthermore, adaptation laws contained within the approaches described above do not guarantee that parameters will converge to their true values, except under special conditions. As such, accurate estimation of subject input is not ensured at all times.

In this paper, we introduce a minimal assist-as-needed (mAAN) controller, which utilizes sensorless force estimation to independently determine subject capability at each moment in time—without assuming any underlying pattern—before providing a corresponding assistance with adjustable ultimate bounds on position error. Our adaptive input estimation scheme employs a Kalman filter (KF) in conjunction with Lyapunov stability analysis and is shown to yield fast, stable, and accurate estimation regardless of subject interaction. Finally, in order to promote active participation of subjects with various capability levels, we introduce two additional algorithms: a bound modification algorithm that alters allowable error and a decayed disturbance rejection algorithm that lets able subjects exceed the desired trajectory. The algorithms are demonstrated experimentally by healthy subjects operating a preexisting rehabilitation robot.

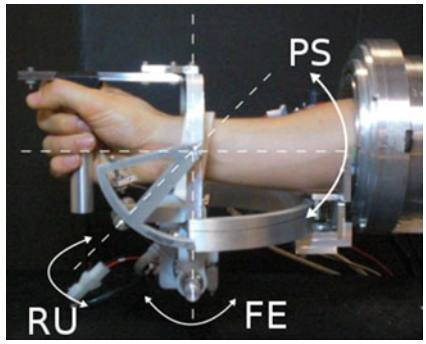

Fig. 1. RiceWrist-S, a robotic rehabilitation device used to experimentally validate our proposed controller. A force sensor was attached at the handle, and unused DOFs (PS & RU) were physically constrained.

This paper is organized as follows. Section II introduces our experimental hardware, Section III derives the sensorless force estimator, and Section IV incorporates that estimation within our proposed control law. Additional algorithms to improve subject adaptivity are detailed in Section V, and the mAAN controller is subsequently tested in Section VI. Finally, the conclusion of our research and remarks for future work are presented in Section VII.

II. Hardware Description and System Modeling

We used the RiceWrist-S [29], a three-degree-of-freedom (DOF) forearm-wrist exoskeleton, as our experimental platform (see Fig. 1). This serial manipulator is capable of independently actuating the user's forearm and wrist DOFs; pronation/supination (PS), flexion/extension (FE), and radial/ulnar deviation (RU) can all be controlled. The RiceWrist-S also incorporates a passive and redundant DOF at the handle to account for any axial misalignments between subject and mechanism.

In order to render low friction and backlash, the device employs both a brushless DC motor to directly drive the PS joint and brushed DC actuators with cable drive transmissions for FE and RU joints. We have previously demonstrated that the RiceWrist-S achieves low apparent inertia, corresponds with the desired range-of-motion, and provides torque outputs appropriate for rehabilitation applications [29].

Our manipulator dynamics can be represented in the traditional form

$$M(q)\ddot{q} + C(q,\dot{q})\dot{q} + g(q) = \tau_r + \tau_p \tag{1}$$

where q is a 3×1 vector of joint positions, M is the 3×3 inertial matrix, C is the 3×3 matrix that represents Coriolis/centrifugal terms, g is the 3×1 gravity vector, τ_r is the 3×1 vector of torques applied by the actuators, and τ_p is the 3×1 vector of torques applied by the subject and mapped into joint space.

We implemented the subsequently proposed mAAN controller on the FE joint of this RiceWrist-S manipulator. Static friction, inertia, and viscous friction have been experimentally identified for this joint. Static friction was estimated from the system response to a ramp position input; inertia and viscous friction were determined by investigating the system response to a step position command. We used the modified logarithmic decrement method presented in [30], which isolates inertial and viscous effects responsible for exponential decay of the system's free vibration.

III. Sensorless Force Estimation

Force sensors can be used to measure the subject's applied force in real time; however, these sensors increase system cost and raise stability concerns [31]. Motivated by a desire to avoid adding force sensors, a variety of "sensorless" force estimation methods employ motors, compliance, or position sensors already incorporated within the robot. Sensorless force estimation techniques exploit differences between the expected and actual manipulator configurations to continuously approximate disturbances applied to the system. Here, we briefly review motor and compliance-based force estimators, before providing a more detailed analysis of model-based force estimation.

For some robots, it is possible to indirectly measure disturbances using motor torques—but motor torques are noisy, particularly if gears are present [32]. Alternatively, this force measurement problem can be converted into a position measurement problem by incorporating compliant elements. Compliance has been implemented at the mechanical level with series elastic actuators [33], and at the controls level via virtual springs [34]. Within the realm of rehabilitation robotics, compliance is particularly attractive because it improves backdrivability and safety during human–robot interaction [35]. Despite these benefits, introducing compliant elements augments design complexity; as such, for systems simply seeking force estimation, compliance might not be the most convenient solution.

In this work, we apply model-based estimation, where plant dynamics and input–output data are used to mathematically extract the disturbance. Given joint positions, velocities, and accelerations, it is trivial to solve the equations of motion for disturbances; in practice, an observer can be used to measure unknown disturbances using incomplete and noisy states. State and disturbance observers are surveyed in [36]. If a robotic manipulator's joint positions and velocities are known, we recommend the well-established nonlinear disturbance observer outlined by Chen *et al.* [37]. Model-based methods are attractive because they 1) provide theoretical guarantees of estimated disturbance accuracy, unlike measured motor torques, and 2) do not mandate design modifications, in contrast with compliant elements.

One drawback of model-based disturbance estimation is that the robot's inertial matrix inverse must typically be calculated. Another flaw is the assumption that disturbances are constant; unless a prediction of future disturbances is available—as might be the case when performing iterative tasks—the resultant estimation trails fluctuating disturbances. Finally, if the plant model is inaccurate, this method cannot correctly distinguish between responses caused by known and unknown inputs; the estimated disturbances therefore include both external forces (τ_p) and unmodeled dynamics (τ_m). While this effect may be undesirable, we will show that model-based disturbance estimation can still be quite convenient. For now, formally denote the disturbance that model-based approaches seek to estimate as

$$d = \tau_p + \tau_m . \tag{2}$$

Applying our disturbance definition, the robot manipulator dynamics (1) can be rewritten as

$$\hat{M}(q)\ddot{q} + \hat{C}(q,\dot{q})\dot{q} + \hat{g}(q) = \tau_r + d. \tag{3}$$

The ensuing paragraphs describe a model-based estimator that yields an approximate disturbance measurement consistent with these equations of motion.

We elected to use a modified version of the sensorless force estimator proposed by Jung *et al.* [38], which employs a KF in conjunction with Lyapunov stability analysis. Since our system measures joint positions but not their derivative, estimation of the system states—i.e., joint position and velocity—is desired alongside force estimation. In the presence of zero-mean white Gaussian noise, KFs minimize the L^2-norm of estimation error; we introduce a KF to address our estimation problem, from which we ultimately derive both a disturbance adaption law and an observer of the aforementioned states. KFs have previously been incorporated in disturbance observers for applications with human–robot interaction [39]. Although dual or joint KFs [40] could have been used for both state and disturbance estimation, interleaving Lyapunov analysis offers an assurance of system stability and safety. Here, we overview the derivation provided by [38] and emphasize our modifications. We will primarily use the variable conventions given in [41], where an intuitive explanation of the KF equations can also be found.

The above nonlinear dynamics (3) converted into stochastic state-space form are posed as

$$\begin{aligned} \dot{x} &= \hat{F}(x)x + \hat{G}(x)\big(\tau_r + d - \hat{g}(x)\big) + n_v \\ y &= Hx + n_w \end{aligned} \tag{4}$$

where $\hat{F}$, $\hat{G}$, and $\hat{g}$ are matrices encoding the estimated dynamic model; $x = (q^T, \dot{q}^T)^T$ is the state vector; y is the measurement vector; n_v is the process noise with covariance Σ_v; and n_w is the sensor noise with covariance Σ_w. The square matrix H maps states to outputs and is presumed to be nonsingular—potentially requiring the use of derivatives and/or integration. KF estimates of the state vector ($\hat{x}$), measurement vector ($\hat{y}$), and error covariance matrix (P) are given by

$$\dot{\hat{x}} = \hat{F}(\hat{x})\hat{x} + \hat{G}(\hat{x})\big(\tau_r + \hat{d} - \hat{g}(\hat{x})\big) - R(\hat{y} - y)$$

$$\begin{aligned}\hat{y} &= H\hat{x} \\ \dot{P} &= \hat{F}(\hat{x})P + P\hat{F}(\hat{x})^T + \Sigma_v - PH^T S^{-1} HP \end{aligned} \tag{5}$$

where $\hat{d}$ is the estimated disturbance vector, R is the weighting matrix between predicted and observed outputs, and P is the solution to the continuous time Riccati equation. According to [41], $R = PH^T S^{-1}$, where S is the residual covariance.

Assume $\hat{F}(x) \approx \hat{F}(\hat{x})$, $\hat{G}(x) \approx \hat{G}(\hat{x})$, and $\hat{g}(x) \approx \hat{g}(\hat{x})$, noting that errors here may lead to bounded stability. This approximation—along with our dynamics formulation—will conveniently facilitate the use of a classical observer, without requiring the linearization applied by Jung *et al.* [38]. Let $e = \hat{x} - x$ and $e_d = \hat{d} - d$; then, use the notation $\bar{e}$ and $\bar{e}_d$ to represent their moving average; by substituting in the state-space representations (4) and (5), we obtain the ensuing dynamic error equation

$$\dot{\bar{e}} = \big(\hat{F}(\hat{x}) - RH\big)\bar{e} + \hat{G}(\hat{x})\bar{e}_d. \tag{6}$$

If $\hat{F}(\hat{x}) - RH$ and $\hat{G}(\hat{x})$ are linearly independent, as is the case for robotic manipulators, a unique equilibrium exists at $\bar{e} = \bar{e}_d = 0$.

Applying Lyapunov stability analysis as described in [42] and [43], this equilibrium is stable when the following conditions are met. Consider the Lyapunov function

$$V_o(e, e_d) = \frac{1}{2}\bar{e}^T \Psi \bar{e} + \frac{1}{2}\bar{e}_d^T \Gamma^{-1} \bar{e}_d \tag{7}$$

where Ψ and Γ are user-selected symmetric positive-definite weighting matrices. Notice we use a constant Ψ rather than the time variant P suggested by Jung *et al.* [38]—including P adds an uncanceled $\dot{P}$ term to the derivative of the Lyapunov function, and hence, the proof found in [38] only applies at steady state ($\dot{P} = 0$). Now, if we compute $\dot{V}_o$ along the trajectories of the system and recall $\dot{d} = 0$, we instead obtain

$$\begin{aligned}\dot{V}_o(e, e_d) = \; & \bar{e}^T \Psi \big(\hat{F}(\hat{x}) - PH^T S^{-1} H\big)\bar{e} \\ & + \bar{e}_d^T \big[\hat{G}(\hat{x})^T \Psi \bar{e} + \Gamma^{-1}\dot{\hat{d}}\big]. \end{aligned} \tag{8}$$

Select the residual covariance inverse and estimated disturbance derivative to be

$$\begin{aligned} S^{-1} &= (H^T)^{-1} P^{-1} \big(\hat{F}(\hat{x}) + \alpha I\big) H^{-1} \\ \dot{\hat{d}} &= -\Gamma \hat{G}(\hat{x})^T \Psi H^{-1} (\hat{y} - y) \end{aligned} \tag{9}$$

where α is a strictly positive constant. Our choice of S^{-1} ensures the matrix $\hat{F}(\hat{x}) - RH$ is stable, while the expression for $\dot{\hat{d}}$ provides an adaption law; plugging (9) back into (8) desirably yields $\dot{V}_o = -\bar{e}^T \alpha \Psi \bar{e}$. Since $\dot{V}_o$ does not contain any $\bar{e}_d$ terms, we can only conclude that $\dot{V}_o$ is negative semi-definite, and hence, the system is stable in the sense of Lyapunov.

A stronger conclusion is attained by recognizing that $\dot{V}_o$ is monotonically decreasing, which implies that V_o, $\bar{e}$, and $\bar{e}_d$ are bounded. Because 1) $\dot{V}_o$ is quadratic in $\bar{e}$, 2) the state estimation error $\bar{e}$ is a square integrable function, and 3) $\dot{\bar{e}}$ is bounded, we can apply Barbalat's Lemma to prove that $\bar{e} \to 0$ as $t \to \infty$. Furthermore, the adaption law converges to true values ($\bar{e}_d \to 0$ as $t \to \infty$) in the presence of certain inputs. Although we will not here detail these necessary excitations, we will demonstrate in Section IV that bounded errors in disturbance estimation are sufficient for our purposes. We, therefore, conclude that both the state and disturbance estimation converge to the moving average of their actual values so long as suitable conditions are met (see Fig. 2).

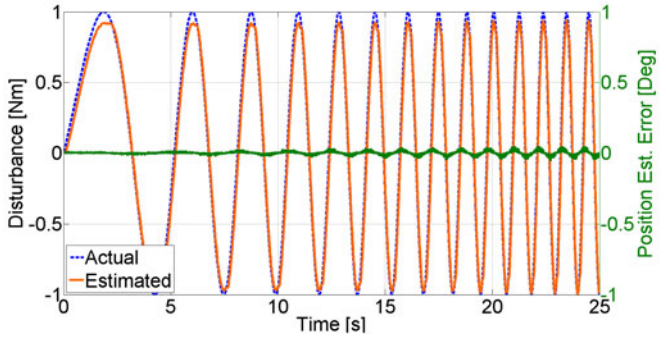

Fig. 2. Disturbance and state measurements found using the proposed sensorless force estimator on a single joint of our RiceWrist-S. The applied torque is a chirp signal sweeping from an initial frequency of 0.1 Hz to a maximum frequency of 1 Hz at 25 s. Position estimation errors were found by subtracting the estimated joint values from the motor's encoder readings. The maximum disturbance estimation error is less than 8% of the disturbance's amplitude, and the position estimation error is always smaller than 0.1°.

During implementation, users will need to tune the gain matrices; fortunately, some intuition can be used to guide the selection of Ψ, Γ, and α. The diagonal indexes of Ψ determine the relative importance of position and velocity estimation errors and affect the corresponding rates of convergence. The magnitude of Γ influences the system's sensitivity to disturbances—diagonal Γ elements can also be biased to vary individual joints' sensitivity. Finally, the constant α acts like the inverse of the sensor noise covariance Σ_w; higher values of α indicate that the sensor readings are more believable, while lower values of α suggest that the model is more accurate. Since the states can often be directly measured through some combination of sensors, derivatives, and/or integration, frequently $H = I$ and the above equations are simplified. In the following sections, we employ this KF with Lyapunov analysis for sensorless force estimation.

IV. Minimal Assist-as-Needed Control Law

We posit that an AAN controller for rehabilitation exercises should 1) help subjects complete desired motions, while 2) encouraging active participation and 3) providing the minimum required assistance [22]. Accordingly, we propose an mAAN controller of the form

$$\tau_r = \tau_b - \hat{d} \tag{10}$$

where τ_b signifies a baseline controller, $\hat{d}$ indicates the model-based disturbance estimate, and τ_r represents the total controller input. This mAAN controller has the same structure as those previously demonstrated in [22] and [23], which both employ a PD baseline controller and feedforward disturbance rejection term. In [22] and [23], the disturbance estimate was found as a function of workspace position—here, however, the subject

forces are dynamically measured without any such positional dependence.

The logic behind this mAAN controller design comes directly from its intended application. If the estimated disturbance is equal to the applied disturbance, then system behavior is governed by a baseline controller; should that baseline controller be designed for trajectory tracking, then "perfect" disturbance rejection ensures desired movements. In practice, sensorless disturbance estimation is never exact (see Section III)—as a result, applied perturbations affect tracking error and hence subject passivity is discouraged. Whenever subjects contribute to a motion, the amount of robotic assistance is reduced accordingly; on the other hand, while subjects are unable to perform a task, the mAAN controller works to offset their applied disturbance. Taken to an extreme, if the subject completes an action flawlessly, then the controller provides no aid—alternatively, if the subject remains inactive, then the controller outputs torques requisite to perform the planned motion, albeit with some tracking error.

Including disturbance rejection within the mAAN controller is theoretically beneficial because it cancels out unknown plant dynamics. Since model-based disturbance estimation considers any deviation from our model as a disturbance, subtracting the resulting estimate drives the plant to behave like our model. Active disturbance rejection control—which has recently garnered considerable attention—relies upon this concept; as argued by Han [44], disturbance rejection transforms the system identification problem into an estimation problem. Depending on the time delay and magnitude of modeling errors, one may purposely select erroneous but desired plant dynamics within a disturbance rejection control scheme so long as the small-gain theorem is upheld [42]. The implications for our mAAN controller are noteworthy—although a correct model is still necessary to purely measure applied torques, slightly incorrect parameterization does not harm closed-loop system performance. This property of disturbance rejection is leveraged within our controller stability analysis.

We selected the passivity-based motion control law proposed by Slotine and Li [45] and detailed in [43] for our baseline controller. Given a twice-differentiable reference trajectory, let us express the position error in joint space as $\tilde{q} = q - q^d$. Define the sliding variables

$$\begin{aligned} v &= \dot{q}^d - \Lambda\tilde{q} \\ a &= \dot{v} \\ r &= \dot{q} - v \end{aligned} \tag{11}$$

where Λ is a positive-definite matrix that determines the weight of position errors relative to velocity errors. The baseline controller can then be written

$$\tau_b = \hat{M}(q)a + \hat{C}(q,\dot{q})v + \hat{g}(q) - K_D r \tag{12}$$

where K_D is a positive-definite gain matrix. The baseline controller, therefore, functions as a PD controller, where K_D and $K_D\Lambda$ serve as the derivative and proportional gains, respectively—rules guiding the selection of K_D are subsequently derived. If desired, this formulation can be converted into task space via the manipulator's kinematics and Jacobian matrix. Implementation of the passivity-based motion controller requires real-time knowledge of the reference trajectory, model dynamics, and system states; these prerequisites do not alter computational demand, however, as 1) the model equations of motion are also solved within the disturbance observer, and 2) the best estimate of joint positions and velocities is found through our KF approach.

Combining our baseline controller (12), mAAN control law (10), and modified manipulator dynamics (3), we obtain

$$\hat{M}(q)\dot{r} + \hat{C}(q,\dot{q})r + K_D r + e_d = 0 \tag{13}$$

Imagine for a moment that $\hat{d}$ is not calculated through estimation, but is precisely measured by some external device. In this idealized case, Lyapunov stability analysis can prove r to be at least uniformly ultimately bounded using the candidate function

$$V_c(r) = \frac{1}{2} r^T M(q) r. \tag{14}$$

Having independently established stability conditions for both the disturbance observer and controlled system, we now seek to verify the stability of our composite controller (10), which integrates $\hat{d}$ estimates from the disturbance observer (9); we here follow the method developed by Chen [46]. Because sensor noise is present, persistent excitations are unassured, and disturbances are time variant, the numerical estimate $\hat{d}$ is inexact—hence, we must also consider controller stability when $e_d \neq 0$.

Choose the Lyapunov candidate function

$$V(e, e_d, r) = V_o(e, e_d) + V_c(r). \tag{15}$$

By taking its time derivative, substituting the robot dynamics, and applying the skew symmetry property, we find

$$\begin{aligned} \dot{V}(e, e_d, r) = \; & -\bar{e}^T \alpha \Psi \bar{e} - r^T K_D r \\ & + r^T \left(\tilde{M}(q)\dot{r} + \tilde{C}(q,\dot{q})r - e_d \right) \end{aligned} \tag{16}$$

where $\tilde{M}(q) = M(q) - \hat{M}(q)$, $\tilde{C}(q,\dot{q}) = C(q,\dot{q}) - \hat{C}(q,\dot{q})$, and $\tilde{g}(q) = g(q) - \hat{g}(q)$. By virtue of our formulation in (3), $\tilde{g}(q)$ is included within e_d. Allow $\|\cdot\|$ to hereafter symbolize the L^2-norm. Using the inequality $y^T x \leq \|y\|\|x\|$ and remembering $\lambda_{\min}(K_D)$ is a lower bound on K_D—where $\lambda_{\min}(K_D)$ denotes the minimum eigenvalue of K_D—it is obvious that $\dot{V}$ can be bounded as

$$\begin{aligned} \dot{V}(e, e_d, r) \leq \; & -\lambda_{\min}(K_D)\|r\|^2 \\ & + \|r\| \cdot \|\tilde{M}(q)\dot{r} + \tilde{C}(q,\dot{q})r - e_d\|. \end{aligned} \tag{17}$$

Let us introduce a constant θ, such that $0 < \theta < 1$, in order to put the previous inequality in the form

$$\begin{aligned} \dot{V}(e, e_d, r) \leq \; & (\theta - 1)\lambda_{\min}(K_D)\|r\|^2 - \theta\lambda_{\min}(K_D)\|r\|^2 \\ & + \|r\| \cdot \|\tilde{M}(q)\dot{r} + \tilde{C}(q,\dot{q})r - e_d\|. \end{aligned} \tag{18}$$

Thus, $\dot{V} \leq (\theta - 1)\lambda_{\min}(K_D)\|r\|^2 \forall r$ if the following inequality is satisfied:

$$\|r\| \geq \frac{\|\tilde{M}(q)\dot{r} + \tilde{C}(q,\dot{q})r - e_d\|}{\theta\lambda_{\min}(K_D)}. \tag{19}$$

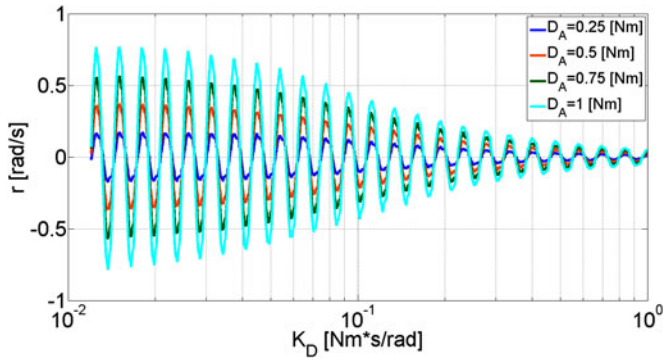

Fig. 3. Tracking error on a single joint of the RiceWrist-S using mAAN control and disturbance observer estimates with both varying K_D values and disturbance amplitudes. Applied torques were sinusoidal, with 1-Hz frequency and amplitude D_A. The robot was commanded to maintain a stationary pose. As K_D increases, the error bounds tighten; here, the amount of error r resulting from an identical input decreases in response to increased K_D. Disturbances with greater amplitude desirably create larger errors.

We, therefore, conclude that the coupled mAAN controller and model-based disturbance estimate yield a tracking error with uniformly ultimately bounded stability (see Fig. 3). A rigorous description of the ultimate bound is made in the Appendix. Should $\tilde{M} \to 0$, $\tilde{C} \to 0$, and $e_d \to 0$, this analysis demonstrates $\|r\| \to 0$ and the system is globally asymptotically stable. Throughout this proof, we assumed $\|r\|$ to be bounded—since the amount of force which a subject can physically realize is naturally limited, it follows that the amount of induced error must be noninfinite. Of particular interest is the inclusion of K_D within the bounded set description; by varying the user-selected gain matrix K_D, we can directly manipulate the bounds on the allowable tracking error. For instance, it may be desirable to decrease the allowable tracking error when subjects are attempting to learn a motion—once those subjects demonstrate proficiency, however, the radius of ultimate boundedness can be increased to challenge subject ability (or vice versa). The mAAN controller presented here is experimentally validated in subsequent sections.

V. Subject-Adaptive Algorithms

By incorporating estimated subject forces within the mAAN controller, we provide minimum required assistance, encourage active participation, and ensure the completion of desired motions; however, unless properly challenged, subjects may still let the robot take control [47]. "Challenge" here refers to difficulty, which implies both the range of acceptable error and degree of robotic assistance. For more impaired subjects, reduced challenges (smaller allowable errors, increased assistance) might be necessary to successfully track trajectories; conversely, less impaired subjects may complete reference movements when greater challenges (larger allowable errors, decreased assistance) are present. The absence of assistance, resistance [48], or even perturbations [49] may best render challenges that promote learning.

In order to adapt challenges to subject capability, we include an algorithm that modulates the allowable error bound based on previous performance. We here exploit the phenomenon that errors combined with visual feedback provide an impetus for active involvement—indeed, error is likely a driving signal for motor learning [50]. Altering error bounds can be interpreted as changing the cross-sectional radius of a desired trajectory; this radius is here modulated according to subject ability. Furthermore, in cases where a subject is consistently able to surpass the desired trajectory, it may be sensible to enable that subject to complete the task in less time than is typically allotted. For this purpose, we have implemented an algorithm, which decays resistive forces when movement speed exceeds the given trajectory. The decay term is continuously altered based on the subject's current ability, without regard to behaviors exhibited during other tasks; contrastingly, the allowable error bound is discretely adjusted between tasks and considers average performance on a task-by-task basis. Viewed together, these subject-adaptive algorithms aim to ensure that all users—regardless of ability—are challenged and therefore encourage active participation for more rapid recovery.

A. Error Bound Modification Algorithm

Since trajectory errors are ultimately bounded by (29), changing the feedback gain K_D modifies allowable error; a high K_D tightens error bounds, while a low K_D relaxes error bounds. We here introduce r^*, a user-specified maximum allowable average trajectory error. By comparing r^* to the current tasks's average error, $\bar{r}_i$, this algorithm updates the feedback gain for the next task, $K_{D,i+1}$. Our formulation is loosely similar to what was detailed in [23], where $K_{D,i+1}$ is computed by 1) comparing the subject's performance to predetermined minimum and maximum average errors and then 2) linearly interpolating between preset feedback gains. Here, however, $K_{D,i+1}$ is modulated in a more direct and responsive manner through both using r^* and accounting for prior performance. More specifically, the algorithm we propose compares $\bar{r}_i$ to $\bar{r}_{i-1}$, the subject's average error during the previous task.

Discrete computation of the feedback gain occurs at the end of each task, and is carried out as

$$K_{D,i+1} = (1 + x_i) K_{D,i} \tag{20}$$

where x_i, the change rate that satisfies $0 < |x_i| < 1$, can be formulated as

$$x_i = x_{\text{nom}} \frac{\bar{r}_i - r^*}{r^*} \left(\frac{|\bar{r}_i - r^*|}{|\bar{r}_{i-1} - r^*|} \right)^{\text{sign}(r^* - \bar{r}_i)} \tag{21}$$

and x_{nom} is a predetermined, constant, nominal change rate. The sign of x_i is determined by comparing the average error in the current task to the maximum allowable error. For example, if $\bar{r}_i$ is smaller than r^*, the algorithm dictates that the subject is able to provide better error performance than expected, and hence, the feedback gain decreases for the subsequent task. The magnitude of x_i depends upon the first and second multiplier terms of x_{nom} in (21); magnitude thus considers both the difference between actual and maximum error and performance changes over time.

Unlike forgetting factors used to alter robotic assistance—for example, [22]—our proposed error bound modification algorithm does not perturb the controller's estimate of subject

capability and strictly regulates the maximum amount of allowable error, yielding more rigorous assurances of stable human–robot interaction. We ultimately feel the algorithm provides clinicians a straightforward means to select what errors are and are not acceptable; hence, our algorithm makes the mAAN controller more suitable for applications in rehabilitation robotics. This algorithm could be adjusted so as to adapt error bounds based on other performance metrics—such as those quantifying movement quality and smoothness—but tracking error was here selected because of its intuitiveness.

B. Disturbance Rejection Decay Algorithm

The error bound modification algorithm constrains users within some radius of the desired trajectory. We next alleviate that constraint by allowing fast intentional movements toward the goal while maintaining the controller's ultimate boundedness characteristics.

In order to reduce resistance of able subjects, we modify the mAAN control law (10). According to this modification, when 1) the subject's position is closer to the target than the desired position, and 2) the subject is inputing force in the target direction, the control law becomes

$$\tau_r = \tau_b - F\hat{d} \tag{22}$$

where F is a decay term that satisfies $0 < F < 1$. This alteration matches with our intuition; if a subject is consistently able to provide force input toward the goal, the controller should be able to allow this "good" disturbance instead of rejecting it. Furthermore, when implementing the disturbance rejection decay algorithm in conjunction with the error bound modification algorithm, $r = 0$ while subjects surpass the reference trajectory.

The decay term F is calculated at every sampling time

$$F_i = (1 + \nu)F_{i-1} \tag{23}$$

where

$$\nu = \begin{cases} \nu_{\text{dec}}, & \text{if } \dot{q}_d \tau_p > 0 \\ \nu_{\text{inc}}, & \text{else} \end{cases} \tag{24}$$

such that $v_{\text{dec}} < 0$ and $v_{\text{inc}} > 0$. The above relationship decreases the term F at a rate of ν_{dec} so long as the subject's force input is in the direction of desired velocity—on the other hand, F increases with a rate of ν_{inc} if the subject reverses input direction. In order to decrease disturbance rejection and move faster than a desired trajectory, consistently correct movement is required. For instance, in a scenario where impaired subjects produce fast but jerky motions, the proposed decay term would balance conflicting tendencies; F here decreases in response to inputs directed toward the goal, but then increases when no torque or erroneous torques are applied. Of course, this algorithm is purely optional and can be omitted in cases where improving movement quality is favored over enabling increased subject participation.

VI. Experiments

We conducted a series of experiments to evaluate the mAAN controller's performance and validate our subject-adaptive algorithms. All experiments were implemented on the FE joint of the RiceWrist-S, which served as a one DOF testbed for the sake of simplicity. The controller was realized using MATLAB/Simulink (The MathWorks, Inc.), and data acquisition at a sampling rate of 1 KHz was achieved using QuaRC (Quanser Inc.). Furthermore, a six-axis nano-17 force sensor (ATI Ind. Autom.) was employed for evaluation purposes. Experiments involving healthy subjects were performed with approval from the Rice University Institutional Review Board.

A. Estimation of Subject Capability

In this experiment, we seek to compare the force estimation quality of the proposed mAAN controller—which is based upon a KF—to widely used adaptive procedures derived from Gaussian RBFs. The control law (10) is executed on the FE joint of the RiceWrist-S for two cases: one where $\hat{d}$ is calculated using our KF approach (9), and a second where $\hat{d}$ is estimated using the RBF procedure.

As indicated in Section I, Gaussian RBFs have been extensively used to model human input for robotic rehabilitation applications [22]–[25]. This approach necessarily assumes subject torque to be strictly position dependent and represents that input as a weighted sum of Gaussian RBFs distributed throughout the motion workspace. Using an adaption law that considers instantaneous position and velocity errors as well as the user's "proximity" to each RBF, this procedure "updates" the RBF weights. For a more detailed description, see [23].

Although position-dependent input torques are presumably present in healthy individuals, the same is not necessarily true for neurologically impaired subjects [26]–[28]. We, therefore, want to evaluate the estimation capabilities of KF and RBF approaches when both position and nonposition-dependent inputs are provided. In order to consistently simulate subject input, an intrinsic disturbance was incorporated as a feedforward term in the controller input. For the first 60 s, that disturbance resisted manipulator movement by acting as a virtual spring; since spring force is directly related to manipulator position, this exemplified a position-dependent torque. After 60 s had elapsed, nonposition-dependent sine-waves with 1.5-, 3.0-, and 4.5-Hz frequencies and 0.05-N·m amplitude were consecutively added at 20-s intervals. The manipulator's desired trajectory was defined as a sine-wave with 0.25-Hz frequency and 20° amplitude. For the Gaussian RBF adaptation, 17 RBFs with 5° function, width were defined throughout the trajectory (in accordance with [23] for a single DOF); we attempted to select parameters that provided the best RBF performance.

Fig. 4 shows the ratio between the L^2 norm of disturbance estimation errors and the L^2 norm of the applied disturbance for both KF and RBF techniques—as well as the L^2-norm of applied non-position dependent disturbances—over 20-s periods. For the first 60 s, the RBFs adapt to position-dependent inputs, and hence, their estimation improves; during the second 60 s, however, that estimation degrades due to the inclusion of nonposition-dependent disturbances, which cannot be accurately modeled because of underlying assumptions in the RBF method. On the other hand, we can see that the KF approach provides relatively constant performance (disturbance

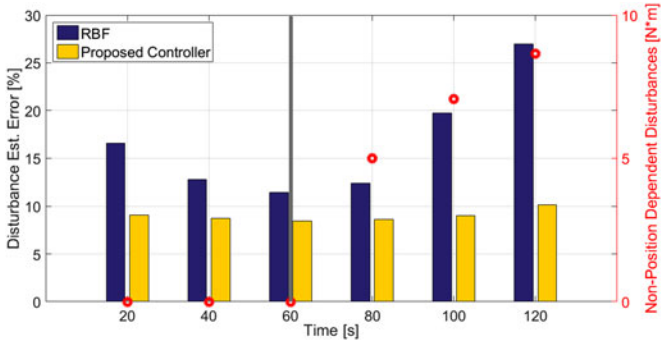

Fig. 4. Comparison of an RBF approach and our proposed mAAN controller during subject input estimation. The bar graph represents the ratio of the L^2 norm of the disturbance estimation error to the L^2 norm of the applied disturbance for both techniques over 20-s intervals. The green dots signify the magnitude of non-position dependent disturbances present over the same intervals—note that non-position dependent disturbances were only added during the second half of this experiment. Parameters for both approaches were selected to provide optimal performance on the FE joint of the RiceWrist-S.

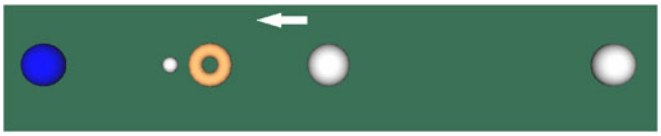

Fig. 5. Visual interface used for human–robot experiments. The torus (orange) represents a subject's actual position, the small ball (white) indicates desired position, and the highlighted sphere (blue) marks our current target. Other spheres (white) correspond with the center and opposite periphery.

estimation errors remain between 8.47% and 10.17%) regardless of whether nonposition-dependent disturbances are present; this indicates that the KF technique is more capable of capturing the range of dynamic behaviors, which may be exhibited by neurologically impaired subjects. We also note that while RBF estimation errors seem to converge toward the KF technique's performance when only position-dependent inputs are present, comparable performance is not achieved within sixty seconds. Through this experiment, we have demonstrated that the force estimation quality of our mAAN controller compares favorably to state-of-the-art Gaussian RBF procedures, both in terms of speed and consistency. We conclude that the proposed mAAN controller is, therefore, better suited to determine subject capability.

B. Validation of the Error Bound Modification Algorithm

We next sought to experimentally examine how the error bound modification algorithm responded to changes in subject involvement; specifically, we aimed to demonstrate that the proposed algorithm can regulate a subject's independence from the exoskeleton. This experiment was performed on the RiceWrist-S with ten healthy subjects, all of which used their dominant arm.

Subjects were instructed to change their involvement strategy during a 180 s series of pointing tasks—"passive" for the first 90 s, then "active" for the second 90 s. Healthy subjects simulated "passive" inability by keeping their hand relaxed while holding the device handle. When "active," subjects moved intentionally to match the desired trajectory; in this segment, a visual display was shown to indicate the actual position, desired trajectory, and randomly assigned target (see Fig. 5).

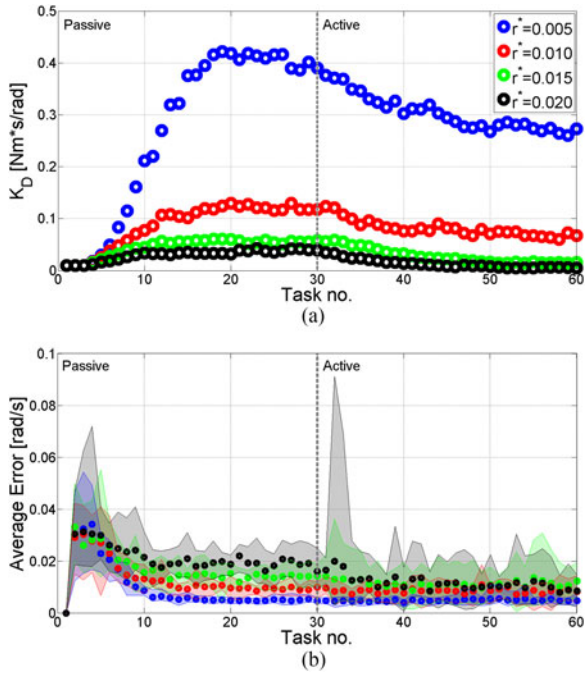

Fig. 6. Effect of error bound modification algorithm on feedback gain and average error. (a) Adapting bounds to subject performance: Feedback gains for passive subjects (task no. 1–30) are higher than for involved subjects (task no. 31–60). As the allowable error decreases, the magnitude of robotic assistance increases. (b) Demonstration of ultimate boundedness: Users are constrained to have an average error less than or equal to r^*. The plotted points represent the mean error across all subjects and the shaded regions depict the corresponding variance. As the bound radius increases, subjects display more independence from the given trajectory.

The total allocated time to move from center-to-periphery and periphery-to-center was 3 s per task. Initial, minimum, and maximum feedback gains were assigned to be 10^{-2}, 10^{-5}, and 0.5 N·m·s/rad, respectively. The feedback gain K_D was updated according to (20) at the end of every task.

The user-specified r^* term employed in (21) defines a maximum allowable average trajectory error; K_D varies in accordance with the relationship between r^* and subject performance. We verified this correlation by testing four different r^* values, ranging from 5×10^{-3} to 2×10^{-2} rad/s, in four subject trials. An r^* value was randomly assigned at the start of each 180 s test, and subjects took breaks between trials in order to minimize fatigue effects.

Fig. 6 depicts the average feedback gain and error as functions of task number (time) and r^* across all ten subjects. Tasks 1–30 (i.e., 0–90 s) correspond with passive interaction, while tasks 31–60 (i.e., 90–180 s) reflect active involvement. Our experimental results in Fig. 6(a) indicate that K_D increased when subjects failed to participate; as the allowable average trajectory error decreased, the feedback gain grew to greater magnitudes in a faster manner. This trend likely stems from (21), where the rate of change for K_D is determined by comparing average trajectory error to r^*. On the other hand, while subjects actively participated K_D decreased with roughly a first-order decay for all assigned r^* values. When r^* was sufficiently small, however, K_D did not approach zero—this is because users were unable to complete the tasks unassisted with an average error less than r^*.

Experimental results shown in Fig. 6(b) demonstrate that error bound adjustments ensured r was less than or equal to r^*. As r^* decreases, more robotic assistance is required even for healthy, active subjects to maintain the desired error level, but when r^* increases above some physically realizable threshold, less assistance is required and subjects are allowed both greater movement variability and independence. The effects of transitioning from passive to active induced noticeable error spikes in cases where the r^* constraints were lessened. Examination of the actuator torque time-series data averaged across all subjects demonstrated that 1) the amount of robotic assistance for passive subjects was uninfluenced by r^* values, and 2) the amount of robotic assistance for active subjects increased as r^* decreased; predictably, greater actuator torques were required for passive tasks than during active participation. We conclude that the error bound modification algorithm can adjust K_D based on subject performance in order to enforce user-specified ultimate bounds.

C. Validation of Disturbance Rejection Decay Algorithm

To demonstrate that the proposed decay algorithm can decrease the rejection of "good" disturbances—i.e., subject inputs directed toward the goal while consistently moving faster than some given trajectory—we conducted an experiment with ten healthy subjects. Subjects were instructed to use their dominant arm and observe the visual feedback presented in Fig. 5. Whenever a target was highlighted, the subject attempted to move toward that goal at a comfortable speed. We specified a desired trajectory that allocated 3 s to move from center-to-periphery and periphery-to-center—this trajectory was designed to be slower than typical subject movements. The initial, minimum, and maximum feedback gains and the r^* value were assigned as 10^{-2}, 10^{-5}, and 0.5 N·m·s/rad and 0.05 rad/s, respectively.

Our mAAN controller was implemented with and without the disturbance rejection decay algorithm in four alternating segments; the decay algorithm was included for segments one and three [shaded gray in Fig. 7(a)], while segments two and four exclusively used the mAAN controller. Each segment was 120 s long. In the first and third segments, the decay term F is modified based on subject performance according to (24). So as to maintain consistency during the experiment, we kept ν_{dec} and ν_{inc} rates constant for all subjects. In practice, these rates could be modulated for subjects with different reaction capabilities.

Examining our experimental results reveals that the disturbance rejection decay algorithm decreased resistive controller actions [see Fig. 7(a)] and allowed subject-defined faster motions [see Fig. 7(b)]. The collective representation of actuator torques given in Fig. 7(a) is supported by time series data, which demonstrates the progression of robotic assistance throughout our experiment. During the first and third segments, the actuator torque magnitude quickly converges to an average value of approximately 0.025 N·m; however, in the second and fourth segments, increased assistance is observed due to constraining controller behavior. We further note that the feedback gain values decrease to the minimum assigned K_D by the end of the first segment and remain at this minimum throughout the rest of the experiment.

Note that during segment transitions, the F term rapidly fluctuates; we believe that this stems from a subject familiarization phase, where in the first segment, users become acquainted with the robotic hardware, and during the third segment, users adapt to the change of controller strategies. Further, since one of the ten participants failed to consistently perform motions faster than the desired trajectory, their atypical data were excluded when constructing Fig. 7(a). Our results demonstrate that including a decay algorithm within the mAAN controller can cater to more able subjects and increases involvement by enabling these users to exceed given trajectories.

VII. Discussion and Conclusion

In this study, we have developed an mAAN controller, which utilizes model-based sensorless force estimation to determine subject capability; by combining a baseline controller with that disturbance estimate, we derived a control law that provides only required aid. The subsequent inclusion of error bound modification and disturbance rejection decay algorithms adapt our controller paradigm to rehabilitation applications and help challenge subjects with various levels of impairment.

Impedance schemes have been frequently employed within the context of AAN control, where their controller properties are modified based on subject performance. Although impedance controllers are easy to implement and possess intuitive properties, these approaches also fail to incorporate the time-varying residual capabilities of a human user and may therefore intervene suboptimally across the robot workspace. To address this issue, adaptive controllers that model the subject's functional capability have been proposed within AAN algorithms. Specifically, Gaussian radial basis networks have been included in adaptive controllers for estimating interaction forces—however, this approach hypothesizes that subject capabilities are position dependent.

We here introduced a model-based estimation method that employs a KF in conjunction with Lyapunov analysis to yield 1) stable estimation of manipulator states and 2) a parameter adaption law that approximates the disturbance derivative. It is shown that, unlike the Gaussian radial basis network approach, this stochastic technique can determine subject inputs that vary spatially and as a function of time; as such, we no longer need to restrictively assume that underlying patterns govern subject capability.

Considering the discovery that error is likely a driving signal for motor learning [50], we implemented an error bound modification algorithm, which leverages the ultimate boundedness of our mAAN controller and modifies the allowable trajectory error via varying a feedback gain. Furthermore, we developed a disturbance rejection decay algorithm that decreases resistive forces when able subject movement desirably exceeds some given trajectory. By means of both improved estimation of subject ability and these challenge algorithms, we hope to increase subject engagement, promote neural plasticity, and better therapy effectiveness—steps that will ultimately reduce treatment duration and cost.

Our sensorless force estimation, error bound modification, and disturbance rejection decay algorithms are all validated experimentally. Results demonstrate that the proposed controller is not limited to estimating only position-dependent subject inputs; furthermore, it is shown that estimation convergence occurs

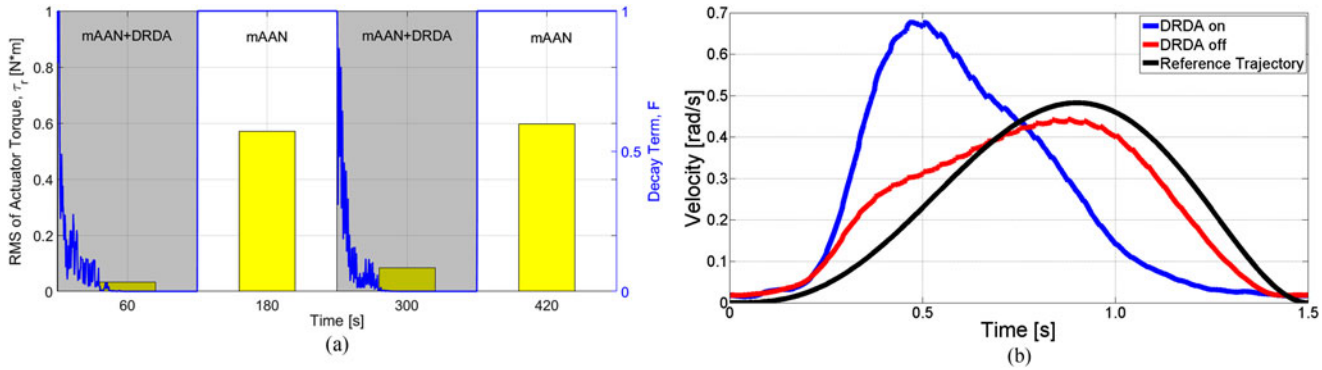

Fig. 7. Controller and subject performance while varying the rejection of "good" disturbances. "DRDA" here indicates the presence of the disturbance rejection decay algorithm. (a) Effect of decay term on controller action: The average decay term F (blue line) and root mean squares of average actuator torques τ_r over 120-s intervals (yellow bars) decrease when subjects consistently demonstrate the capability to correctly surpass a given trajectory. (b) Average trajectories with and without the decay algorithm: Permitting able movements allows the subject to more quickly attain the target position and therefore encourages involvement.

much faster than the Gaussian radial basis network approach—for example, in Fig. 4, the norm estimation error for our proposed controller was approximately half the norm estimation error of an RBF controller. Experiments with healthy subjects verify that the error bound modification is capable of responding to changes in involvement. Inclusion of an upper bound on the average allowable error enables explicit definition of acceptable movement variability and subject–robot independence. Experiments also show that the disturbance rejection decay algorithm encourages voluntary movement by decreasing input rejection when subject forces are 1) consistently directed toward the goal and 2) of greater magnitude than strictly required for trajectory following. In this situation, subjects are allowed to define a pace different from the externally imposed reference trajectory.

Future work includes testing the mAAN controller in a clinical setting for the rehabilitation of neurologically impaired subjects. Tuning here should be straightforward—therapists can use r^* to select an appropriate error bound radius, and switch F based on whether trajectory following or increased variability tasks are desired. Ideally, we would like to compare recovery induced by our mAAN controller with results obtained by other AAN control approaches; we also want to examine how r^* and F tools are best utilized by practitioners. Clinicians might consider the implementation strategy of this controller; specifically, either tuning parameters individually for each joint space DOF, or adopting parameters based on coordinated movements in task space. While for unimpaired subjects there exists some evidence [51] to support training of coordinated movements through decomposition into joint space motions—such as the wrist FE movement used in our experimental validation—there remains a lack of evidence within neurologically impaired populations [52] to favor this technique over directly training coordinated movements. The inclusion of an algorithm that modulates allocated time based on subject performance may be a further addition to the described controller.

APPENDIX

Although the proposed Lyapunov function (15) depends on multiple states, we here aim to define an upper bound for the trajectory error r. The inequality identified in (19) enables us to conclude that the trajectory error r is uniformly ultimately bounded; this ultimate bound on trajectory error can be explicitly calculated with the following bounding class κ functions, which are always possible to find [42]:

$$\alpha_1(\|r\|) \leq V(e, e_d, r) \leq \alpha_2(\|r\|). \tag{25}$$

The ultimate bound B_u on trajectory error r can be defined in a rather conservative way [42] as

$$B_u = \alpha_1^{-1}\big(\alpha_2(\|\mu\|)\big) \tag{26}$$

where μ is the limiting term that satisfies $\dot{V} < 0 \ \forall \|r\| \geq \mu \geq 0$.

The stability analysis described via (7)–(9) indicates that the state estimation error e and disturbance estimation error e_d are bounded and enables us to define an upper bound as

$$\frac{1}{2}\bar{e}^T \Psi \bar{e} + \frac{1}{2}\bar{e}_d^T \Gamma^{-1} \bar{e}_d \leq D. \tag{27}$$

The bounding functions of the Lyapunov function (15) can be identified considering both the relation given in (27) and the fact that the inertia matrix itself is both positive definite and bounded [53]. Hence, the subsequent inequality can be written for the proposed Lyapunov function

$$\frac{1}{2}\lambda_{\min}(M)\|r\|^2 \leq V(e, e_d, r) \leq \frac{1}{2}\lambda_{\max}(M)\|r\|^2 + D \tag{28}$$

where $\lambda_{\min}$ and $\lambda_{\max}$ are the minimum and maximum eigenvalues of inertia matrix M throughout a given workspace. We note that the left and right sides of (28) correspond to $\alpha_1(\|r\|)$ and $\alpha_2(\|r\|)$, respectively. By using the right-hand side of the inequality (19) as the limiting term μ and utilizing the bounding functions defined in (28), the ultimate bound on the trajectory error r can be calculated via (26)

$$B_u = \sqrt{\frac{\lambda_{\max}(M)\|\tilde{M}(q)\dot{r} + \tilde{C}(q, \dot{q})r - e_d\|^2 + D}{\lambda_{\min}(M)\theta^2 \lambda_{\min}^2(K_D)}}. \tag{29}$$

REFERENCES

[1] D. Mozaffarian *et al.*, "Heart disease and stroke statistics—2015 update: A report from the American Heart Association," *Circulation*, vol. 131, pp. e151–e177, 2015.

[2] National Spinal Cord Injury Statistical Center, "Spinal cord injury (SCI) facts and figures at a glance," 2015.
[3] M. Berkowitz, *Spinal Cord Injury: An Analysis of Medical and Social Costs*. New York, NY, USA: Demos Medical Pub, 1998.
[4] R. Riener, T. Nef, and G. Colombo, "Robot-aided neurorehabilitation of the upper extremities," *Med. Biol. Eng. Comput.*, vol. 43, no. 1, pp. 2–10, 2005.
[5] C. Bütefisch *et al.*, "Repetitive training of isolated movements improves the outcome of motor rehabilitation of the centrally paretic hand," *J. Neurol. Sci.*, vol. 130, no. 1, pp. 59–68, 1995.
[6] A. Frisoli *et al.*, "Arm rehabilitation with a robotic exoskeleleton in virtual reality," in *Proc. IEEE Int. Conf. Rehabil. Robot.*, 2007, pp. 631–642.
[7] A. C. Lo *et al.*, "Robot-assisted therapy for long-term upper-limb impairment after stroke," *New England J. Med.*, vol. 362, no. 19, pp. 1772–1783, 2010.
[8] N. Yozbatiran *et al.*, "Robotic training and clinical assessment of upper extremity movements after spinal cord injury: A single case report," *J. Rehabil. Med.*, vol. 44, no. 2, pp. 186–188, 2012.
[9] L. Marchal-Crespo and D. Reinkensmeyer, "Review of control strategies for robotic movement training after neurologic injury," *J. Neuroeng. Rehabil.*, vol. 6, no. 1, pp. 1–15, 2009.
[10] A. Basteris *et al.*, "Training modalities in robot-mediated upper limb rehabilitation in stroke: A framework for classification based on a systematic review," *J. Neuroeng. Rehabil.*, vol. 11, p. 111, 2014.
[11] Z. Warraich and J. A. Kleim, "Neural plasticity: The biological substrate for neurorehabilitation," *PM&R*, vol. 2, no. 12, pp. S208–S219, 2010.
[12] N. Hogan, "Impedance control: An approach to manipulation," *J. Dyn. Syst. Meas. Control*, vol. 107, no. 1, pp. 1–24, 1985.
[13] H. I. Krebs *et al.*, "Rehabilitation robotics: Performance-based progressive robot-assisted therapy," *Auton. Robots*, vol. 15, pp. 7–20, 2003.
[14] Y. Mao and S. K. Agrawal, "Design of a cable-driven arm exoskeleton (CAREX) for neural rehabilitation," *IEEE Trans. Robot.*, vol. 28, no. 4, pp. 922–931, Aug. 2012.
[15] M. Mihelj, T. Nef, and R. Riener, "A novel paradigm for patient-cooperative control of upper-limb rehabilitation robots," *Adv. Robot.*, vol. 21, no. 8, pp. 843–867, 2007.
[16] J. L. Emken, J. E. Bobrow, and D. J. Reinkensmeyer, "Robotic movement training as an optimization problem: Designing a controller that assists only as needed," in *Proc. IEEE Int. Conf. Rehabil. Robot.*, 2005, pp. 307–312.
[17] R. Wei *et al.*, "Adaptive iterative learning control design for RUPERT IV," in *Proc. IEEE RAS EMBS Int. Conf. Biomed. Robot. Biomechatron.*, 2008, pp. 647–652.
[18] T. Proietti *et al.*, "Adaptive control of a robotic exoskeleton for neurorehabilitation," in *Proc. IEEE/EMBS Int. Conf. Neural Eng.*, 2015, pp. 803–806.
[19] F. Girosi and T. Poggio, "Networks and the best approximation property," *Biol. Cybern.*, vol. 63, no. 3, pp. 169–176, 1990.
[20] R. M. Sanner and J.-J. E. Slotine, "Gaussian networks for direct adaptive control," *IEEE Trans. Neural Netw.*, vol. 3, no. 6, pp. 837–863, Nov. 1992.
[21] R. M. Sanner and M. Kosha, "A mathematical model of the adaptive control of human arm motions," *Biol. Cybern.*, vol. 80, no. 5, pp. 369–382, 1999.
[22] E. T. Wolbrecht *et al.*, "Optimizing compliant, model-based robotic assistance to promote neurorehabilitation," *IEEE Trans. Neural Syst. Rehabil. Eng.*, vol. 16, no. 3, pp. 286–297, Jun. 2008.
[23] A. U. Pehlivan, F. Sergi, and M. K. O'Malley, "A subject-adaptive controller for wrist robotic rehabilitation," *IEEE Trans. Mechatronics*, vol. 20, no. 3, pp. 1338–1350, Jun. 2015.
[24] C. Bower, H. Taheri, and E. Wolbrecht, "Adaptive control with state-dependent modeling of patient impairment for robotic movement therapy," in *Proc. IEEE Int. Conf. Rehabil. Robot.*, 2013, pp. 1–6.
[25] M. Guidali *et al.*, "Online learning and adaptation of patient support during ADL training," in *Proc. IEEE Int. Conf. Rehabil. Robot.*, 2011, pp. 1–6.
[26] A. Handley *et al.*, "Movement disorders after stroke," *Age Ageing*, vol. 38, no. 3, pp. 260–266, 2009.
[27] M. O. Conrad and D. G. Kamper, "Isokinetic strength and power deficits in the hand following stroke," *Clin. Neurophysiol.*, vol. 123, no. 6, pp. 1200–1206, 2012.
[28] P. S. Lum *et al.*, "Effects of velocity on maximal torque production in poststroke hemiparesis," *Muscle Nerve*, vol. 30, no. 6, pp. 732–742, 2004.
[29] A. U. Pehlivan *et al.*, "Design and validation of the RiceWrist-S exoskeleton for robotic rehabilitation after incomplete spinal cord injury," *Robotica*, vol. 32, no. 8, pp. 1415–1431, 2014.
[30] J. Liang and B. Feeny, "Identifying coulomb and viscous friction from free-vibration decrements," *Nonlinear Dyn.*, vol. 16, pp. 337–347, 1998.
[31] C. H. An and J. M. Hollerbach, "Dynamic stability issues in force control of manipulators," in *Proc. Am. Control Conf.*, 1987, pp. 821–827.
[32] J. Swevers *et al.*, "Optimal robot excitation and identification," *IEEE Trans. Robot. Autom.*, vol. 13, no. 5, pp. 730–740, Oct. 1997.
[33] G. A. Pratt and M. M. Williamson, "Series elastic actuators," in *Proc. IEEE/RSJ Int. Conf. Intell. Robots Syst.*, 1995, vol. 1, pp. 399–406.
[34] A. Stolt *et al.*, "Force controlled robotic assembly without a force sensor," in *Proc. IEEE Int. Conf. Robot. Autom.*, 2012, pp. 1538–1543.
[35] H. Vallery *et al.*, "Compliant actuation of rehabilitation robots," *IEEE Robot. Autom. Mag.*, vol. 15, no. 3, pp. 60–69, Sep. 2008.
[36] A. Radke and Z. Gao, "A survey of state and disturbance observers for practitioners," in *Proc. Am. Control Conf.*, 2006, pp. 5183–5188.
[37] W.-H. Chen *et al.*, "A nonlinear disturbance observer for robotic manipulators," *IEEE Trans. Ind. Electron.*, vol. 47, no. 4, pp. 932–938, Aug. 2000.
[38] J. Jung, J. Lee, and K. Huh, "Robust contact force estimation for robot manipulators in three-dimensional space," *Proc. Inst. Mech. Eng. C, J. Mech. Eng. Sci.*, vol. 220, no. 9, pp. 1317–1327, 2006.
[39] C. Mitsantisuk, S. Katsura, and K. Ohishi, "Kalman-filter-based sensor integration of variable power assist control based on human stiffness estimation," *IEEE Trans. Ind. Electron.*, vol. 56, no. 10, pp. 3897–3905, Oct. 2009.
[40] E. A. Wan and A. T. Nelson, "Dual extended Kalman filter methods," in *Kalman Filtering and Neural Networks*, S. S. Haykin, Ed. New York, NY, USA: Wiley, 2001, pp. 123–173.
[41] H. Choset, *et al.*, *Principles of Robot Motion: Theory, Algorithms, and Implementation*. Boston, MA, USA: MIT Press, 2005.
[42] H. K. Khalil and J. Grizzle, *Nonlinear Systems*, vol. 3. Upper Saddle River, NJ, USA: Prentice-Hall, 2002.
[43] M. W. Spong, S. Hutchinson, and M. Vidyasagar, *Robot Modeling and Control*, vol. 3. New York, NY, USA: Wiley, 2006.
[44] J. Han, "From PID to active disturbance rejection control," *IEEE Trans. Ind. Electron.*, vol. 56, no. 3, pp. 900–906, Mar. 2009.
[45] J.-J. E. Slotine and W. Li, "On the adaptive control of robot manipulators," *Int. J. Robot. Res.*, vol. 6, no. 3, pp. 49–59, 1987.
[46] W.-H. Chen, "Disturbance observer based control for nonlinear systems," *IEEE Trans. Mechatronics*, vol. 9, no. 4, pp. 706–710, Dec. 2004.
[47] E. T. Wolbrecht, "Adaptive, assist-as-needed control of a pneumatic orthosis for optimizing robotic movement therapy following stroke," Ph.D. dissertation, Univ. California, Irvine, CA, USA, 2007.
[48] K. D. Fitle, A. U. Pehlivan, and M. K. O'Malley, "A robotic exoskeleton for rehabilitation and assessment of the upper limb following incomplete spinal cord injury," in *Proc. IEEE Int. Conf. Robot. Autom.*, 2015, pp. 4960–4966.
[49] J. L. Patton *et al.*, "Evaluation of robotic training forces that either enhance or reduce error in chronic hemiparetic stroke survivors," *Exp. Brain Res.*, vol. 168, no. 3, pp. 368–383, 2006.
[50] S. G. Lisberger, "The neural basis for learning of simple motor skills," *Science*, vol. 242, no. 4879, pp. 728–735, 1988.
[51] J. Klein, S. J. Spencer, and D. J. Reinkensmeyer, "Breaking it down is better: Haptic decomposition of complex movements aids in robot-assisted motor learning," *IEEE Trans. Neural Syst. Rehabil. Eng.*, vol. 20, no. 3, pp. 268–275, May 2012.
[52] M.-H. Milot *et al.*, "A crossover pilot study evaluating the functional outcomes of two different types of robotic movement training in chronic stroke survivors using the arm exoskeleton BONES," *J. Neuroeng. Rehabil.*, vol. 10, p. 112, 2013.
[53] F. Ghorbel, B. Srinivasan, and M. W. Spong, "On the positive definiteness and uniform boundedness of the inertia matrix of robot manipulators," in *Proc. IEEE Conf. Decision Control*, 1993, pp. 1103–1108.

Ali Utku Pehlivan (S'11) received the B.S. degree in mechatronics engineering from Sabanci University, Istanbul, Turkey, in 2009, and the M.S. degree in mechanical engineering from Rice University, Houston, TX, USA, in 2012. He is currently working toward the Ph.D. degree with the Mechanical Engineering Department, Rice University, as a Member of Mechatronics and Haptic Interfaces Laboratory.

His research interests include design of wearable robotic manipulators, human–robot interaction for robot-aided neurorehabilitation, nonlinear control, mechatronics, and robotics.

Dylan P. Losey (S'14) received the B.S. degree in mechanical engineering from Vanderbilt University, Nashville, TN, USA, in 2014. Since then, he has been working toward the Ph.D. degree in mechanical engineering with Rice University, Houston, TX, USA, as a Member of the Mechatronics and Haptic Interfaces Laboratory.

His research interests include human–robot interaction and machine learning.

Mr. Losey received an NSF Graduate Research Fellowship in 2014.

Marcia K. O'Malley (SM'13) the B.S. degree in mechanical engineering from Purdue University, West Lafayette, IN, USA, in 1996, and the M.S. and Ph.D. degrees in mechanical engineering from Vanderbilt University, Nashville, TN, USA, in 1999 and 2001, respectively.

She is currently a Professor of mechanical engineering and of computer science at Rice University, Houston, TX, USA, and directs the Mechatronics and Haptic Interfaces Laboratory. She is adjunct faculty in the Departments of Physical Medicine and Rehabilitation at the Baylor College of Medicine and the University of Texas Medical School at Houston, and is the Director of Rehabilitation Engineering at TIRR-Memorial Hermann Hospital. Her research addresses issues that arise when humans physically interact with robotic systems, with a focus on training and rehabilitation in virtual environments.

Prof. O'Malley is a Fellow of the American Society of Mechanical Engineers and serves as an Associate Editor for the *ASME Journal of Mechanisms and Robotics*.